SI Appendix materials

Materials and Methods

Generation of miR-183 cluster knockout mice: All mice involved in this study were handled according to the NIH animal care and use guidelines.

Deletion of the miR-183 cluster locus, a 3.82kb genomic region between Nrf1 and Ub2eh genes (chr6 qA3.3)(S2A&E), was achieved through homologous recombination in R1 ES cells (129SV6) as described elsewhere (S2A&E) (1). Briefly, a replacement type gene targeting vector was constructed from a SV129 BAC clone covering the mouse chr6:30,103,463-30,161,298 genomic region through ET recombination (S2A) (2). Linearized targeting vector was electroporated into the R1 ES cells; and HR events, enriched by the presence of Diphtheria Toxin A (DTA) in the targeting vector (S2A), were confirmed by Southern blotting by the presence of either a 7.813kb EcoRI band (EcoRI KO allele, shown in S2B) with a 3' probe or a 6.17k BamHI band (BamHI KO allele, not shown) with a 5' probe (S2A). Correctly recombined ES clones were microinjected into blastocysts of C57BL/6J. The miR-183 cluster knockout allele, designated as miR-183 cluster-KO, was transmitted through germline successfully and further brought into the C57B/6J background through subsequent 5 or more generations of breeding before phenotypic evaluations. Floxed Neo cassette was removed by crossing with the germline Cre strain ZP3-Cre (3). For genotyping of the targeted allele, genomic DNA from tail clips were isolated with DNEasy Blood & Tissue Kit (Qiagen, Valencia, CA) and PCR reactions were carried out using the following primer pairs: 5'-GCCACCCTGGAGCAAGGCTGGATCCCAAGT-3' and 5'-GTTGGCGCCTACCGGTGGATGTGGAATGTGT-3' for the miR-183 cluster-KO allele (436 bp) and 5'-GCCACCCTGGAGCAAGGCTGGATCCCAAGT-3' and 5'-CTGGTCTGGCTGCTGGAGGCCTCCC-3' for the corresponding wild type allele (319 bp).

Northern blotting: Northern hybridization was carried out according to an established protocol (S1A; S2C)(4). Briefly, small RNA-enriched total RNAs were isolated from tissues of adult mice using the miRNeasy Micro Kit (Qiagen) with manufacturer suggested procedures. Three to 15 µg of total RNA samples were fractioned in a precast 15% denaturing polyacrylamide gel containing 6M urea in TBE (Invitrogen) by electrophoresis, and transferred to the positively charged Nylon GeneScreen membrane (Perkin Elmer) in 20X SSC overnight. Blotted RNA was fixed by UV cross-

linking to the membrane. LNA spiked-oligo nucleotide probes, specific to miR-183 (5'-AGTGAATTCTACCAGTGCCATA-3'), miR-96 (5'- AGCAAAAATGTGCTAGTGCCAAA-3') and miR-182 (5'-CGGTGTGAGTTCTACCATTGCCAAA-3') respectively (Exiqon), were end-labeled with [γ-P32] ATP (Perkin Elmer) by T4 kinase (Invitrogen) as described (4). The blotted membranes were hybridized to LNA probes in PerfectHyb Plus hybridization solution (Sigma) overnight at 68°C and washed twice in 2X SSC at the hybridization temperature. Signals were collected onto a phosphor imaging screen and visualized on a Typhoon Scanner (Fuji) with the ImageQuant software.

RT-PCR and qPCR analysis: Total RNA was extracted using miRNeasy Mini Kit (Qiagen). For mRNA detection and analysis, 400 ng RNA per sample was reverse transcribed using SuperScript III reverse transcriptase (Invitrogen) with a mixture of oligo(dT) and random hexamers. Quantitative PCR (qPCR) was performed using a FastStart SYBR Green Master (Roche), and expressions of genes of interests were analyzed with appropriate reference genes pre-selected by using Genorm (http://www.biogazelle.com/genormplus). For mature microRNAs (miR-96, 182, and 183) detection and analysis, the miScript Reverse Transcription Kit (Qiagen) was used to carry out reverse transcription and real time qRT-PCR was performed using the miScript SYBR Green PCR kit with miScript Universal primer and the predesigned miScript Primer assay (Qiagen).

Immunohistochemistry: Mouse eyes were marked with blue dye on the ventral side before removal from the euthanized mice, and embedded in Optimal Cutting Temperature (OCT) (Tissue-Tek, Torrance, CA) with appropriate orientation so that the ventral-dorsal sections of retina were collected. Frozen sections (10 µm thickness) were permeabilized in PBS containing 0.2% Triton X-100 for 15 min at room temperature, washed 3x in PBS, and blocked with ICC buffer (1x PBS with 0.2 % Tween-20, 0.5% bovine serum albumin (BSA) and 0.05% sodium azide) containing 10% goat serum for 2 hours at room temperature. After washing 1x with PBS, the sections were incubated with primary antibodies in ICC buffer with 10% goat serum for 3 hours at room temperature, washed 3x with ICC buffer (10 min each) and then incubated with secondary antibodies with DAPI (1 µg/ml) in ICC buffer for 1 hour at room temperature. The sections were washed 3x in ICC buffer for 10 min each and 2x with PBS for 15 min each and

then mounted in Prolong Gold mounting media (Invitrogen) before imaging on Olympus FV1000 confocal microscope.

Antibodies used for immunostaining are included in the following table:

Antibody	Species	Working dilution	Source
S-opsin	goat	1:100,	Santa Cruz sc-14363
M-opsin	rabbit	1:1000,	Millipore. AB5405
mCAR	rabbit	1:1000,	Millipore. AB15282
Rhodopsin	mouse	1:5000,	Millipore. MAB5316
Glutamylated-tubulin (GT355)	mouse	1:500,	Adipogen AG-20B-0020
Chx10	Sheep	1:200,	Abcam, ab16142
PKCα	Mouse	1:1000,	Sigma, p5704
GFAP	Rabbit	1:1000,	A gift from Anand Swaroop
Brn3a	Mouse	1:20,	A gift from Tudor Badea
Calbindin	Rabbit	1:1000,	Millipore, MAB1778
Rootletin	Rabbit	1:1000,	(5)
Rp1	Chick	1:2000,	A gift from Qin Liu (MEEI)
Myo7a	Rabbit	1:1000,	Invitrogen, PA1-936
Zo-1	Rabbit	1:500,	Millipore, AB2272
acetylated α-tubulin	Mouse	1:800,	Sigma, cat # T6593
Pax6	Rabbit	1:1000,	A gift from Anand Swaroop
OMP	Mouse	1:5000,	Wako, 544-1001
Gap-43	Rabbit	1:2500,	Novus, NB300-143

Luciferase reporter assay: HEK293 cells were plated 24 hours before transfection at a density of 0.5×10^5 cells/well in 24-well plates. Fifty ng of a luciferase-expressing vector harboring the 3'UTR from Mak gene was cotransfected with 10 pmoles mimics (LNA oligos) of miR-183 cluster member miRNAs at a molar ratio of miR-182:miR-183:miR-96=1:1:2 (Exiqon, MA) with or without inhibitors (LNA oligos). Thirty six hours after transfection, the firefly and Renilla luciferase

activities were determined by luminometer readings using Dual-Luciferase Reporter Assay systems (Promega, Madison, WI, USA).

ERG recording: ERGs were recorded using the Diagnosys Espion E2 Electrophysiology System (Diagnosys, Lowell, MA). Mice were dark adapted for 16 hours before ERG test. After anesthesia by intraperitoneal injection of ketamine (100 mg/kg body weight) and xylazine (6 mg/kg body weight), pupils were dilated with tropicamide (1%) and phenylephrine hydrochloride (2.5%), and corneas were anesthetized with proparacaine (1%). Gonak™ Hypromellose Solution, 2.5% (Akorn Incorporated) was used to maintain corneal hydration and electrical contact. The ERG was recorded with a gold electrode placed on the center of cornea, a reference electrode placed in the mouth and the background electrode inserted under the skin near the tail. Mouse body temperature was maintained using a heated rodent table set at 37 ˚C (Diagnosys LLC). Light stimulus was provided by attached ColorDome. For dark-adapted responses, stimulus flash intensity varied from –4.0 to 1 log sc cd·s/m^2 with inter-stimulus interval of 10 to 60 seconds. Light-adapted ERG responses were obtained with the presence of a rod-saturating background light. Flash intensity varied from -0.52 to 2 log sc cd·s/m^2 in 6 steps, and responses elicit at each light intensity were averaged 20 times.

Auditory brainstem response (ABR) test: ABR tests were performed as described (6). Briefly, pure-tone stimuli were generated with the SmartEP (Intelligent Hearing Systems (IHS)) software and presented through a high-frequency transducer. ABR waveforms were elicited using rarefaction polarity tone bursts of 8, 16, 24, and 32 kHz at a rate of 21.1 per second. Tone burst stimuli were 3 ms in duration and shaped using a Blackman envelope. ABR testing was performed at approximately 3 months age on four wild type, five heterozygous and two homozygous littermates. Mice were anesthetized with an intraperitoneal injection of a combination of 56mg/kg body weight of ketamine (Vedco) and 0.375mg/kg body weight of dexdomitor (Pfizer). Mice were maintained at 37°C during testing in a sound-proof booth (Acoustic Systems). To record auditory brainstem potentials, sterile subdermal needle electrodes were used, with one applied to the forehead, and one each behind the left and right pinnae. The right ear only was tested for each animal. The stimulus intensity began at 100 dB SPL and was decreased in 10-dB

steps until no ABR waveform could be seen. The procedure was repeated with 5-dB step decreases as threshold was approached, until the lowest level replicable response was obtained, which was then considered to be threshold. After all threshold data were obtained for each tone burst stimulus, mice were administered a 0.01 ml/gram body weight dose of antisedan (Pfizer) and placed in a heated recovery cage. Waveforms elicited by 16-kHz stimuli at 90 dB SPL were used to determine absolute and interpeak latencies. Thresholds were compared using 2-way ANOVA unweighted means analysis with within-frequency post-test comparisons to heterozygote means corrected for multiple testing**.**

Buried food assay: Olfactory detection was assessed by the Buried Food assay (7). For two consecutive days before the test, animals were singly housed and a single Goldfish cracker (Pepperidge Farm) was placed in each cage. To ensure palatability, cages were checked the next day to ensure each mouse had consumed the cracker. Before the test, mice were food-deprived for 24 h. During the test, a mouse was placed in the test cage (46 cm L × 23.5 cm W × 20 cm H) containing 3.5 cm of clean bedding for 5 minutes to acclimate to the cage. Then the mouse was removed from the test cage, and a cracker was buried under the bedding on the bottom of the cage at a random location. The mouse was reintroduced to the test cage, and the time taken to retrieve the cracker was recorded. If mice failed to find the buried cracker after 10 minutes had elapsed, mice were determined to have failed the test and 600 seconds was recorded as the latency score. Mice who failed the test were re-tested with a visible cookie to ensure mice were sufficiently motivated by hunger. Subjects were 8-10 weeks old male mice (n=10 miR-183 cluster$^{ko/ko}$, 14 miR-183 cluster$^{ko/+}$, and 9 miR-183 cluster$^{+/+}$. Results were analyzed with an ordinary one-way ANOVA in GraphPad Prism. A Tukey test was used for post-hoc analysis.

Light and transmission electron microscopy: Mouse eyes, after being marked with a blue tissue marking dye (Polysciences Inc., Warrington, PA) on the ventral side, were removed from mice and placed immediately in fixative (2.5% glutaraldehyde (GA) + 2% paraformaldehyde (PFA) in PBS) on ice. After fixation for 60 minutes, the front of the eye was cut open under a dissecting microscope (Zeiss Stemi 2000-C, Carl Zeiss, Thornwood, New York) with a micro-scissors by removing a small piece of the cornea at the center and fixation continued for another 3-4 h at

4˚C. The entire cornea except for a small area at the marked ventral side was excised, the lens was removed and the eye cup continued to be fixed for another 24 h at 4 ˚C. Fixed samples were washed and post fixed with 2% OsO4 (Electron Microscopy Sciences (EMS), Hatfield, PA) in PBS (0.3 ml per eye cup in 48 well plates) for two hours on ice in a fume hood. After complete removal of OsO4, the osmicated tissues were washed again, dehydrated sequentially and infiltrated in Embed 812, DDSA, NMA, BDMA in a volume ratio of 40:25:20:2 (EMS) according to manufacturer's standard protocol. Tissues were then transferred to a rubber mold filled with fresh embedding medium. Tissues were oriented with the uncut cornea tissue (the ventral side of retina) positioned at the bottom under a dissecting microscope, allowing proper dorsal-ventral orientation. After becoming completely hardened at 60^{o}C (36-48 hours), the blocks were trimmed to the optic nerve head (center of retina) and semi-thin (500 nm thickness) and ultra-thin (70-90 nm thickness) sections were cut with a histo- or ultra-diamond knife (Diatome-U.S., Hatfield, PA), respectively. For light microscopy, the semi-thin sections were stained with the Azure B-Methylene Blue-Toluidine Blue dye mixture (at 0.25% for each dye in 0.25% sodium borate) and imaged with a Nikon Eclipse E800 light microscope (Nikon USA, Melville, NY). For electron microscopy, the ultra-thin sections were counter stained sequentially with 1% uranyl acetate and 2.7% lead citrate before being imaged with a Joel 1010 Transmission Electron Microscope equipped with an AMT (5 MP) digital camera system (JEOL USA, Peabody, MA).

Thickness of Retinal Layers and Cone Nuclei Counting: Plastic sections (500 nm thickness) spanning entire retina from dorsal to ventral were imaged with 20x objective lens using Nikon Eclipse E800 microscope. Thickness of retinal layers at different locations relative to the optical nerve head (ONH) was measured using the AxioVision software (Carl Zeiss, Oberkochen, Germany).

Scanning electron microscopy: The inner ear was removed from experimental mice, and a small hole made at the top of the cochlea with the tip of a fine forceps. The inner ear was gently flushed with ~0.3 ml of 2.5% glutaraldehyde fixative solution for 2 h at room temperature. The membranous labyrinth containing the cochlea and vestibular end organs was removed by dissection. Specimens were processed using three 1 h incubations with 1% (w/v) OsO4,

alternated with two 1 h incubations in 1% tannic acid (w/v). The specimens were then dehydrated with a graded ethanol series and critical point dried using liquid CO2 as the transitional fluid. Samples were sputter coated with carbon and platinum and viewed using a Hitachi S-4800 field-emission scanning electron microscope operated at 5 kV.

Cochlea Tissue dissection and immunostaining: Temporal bones were isolated from postnatal mice and fixed in 2-4% paraformaldehyde at 4ºC for 2 hours. Following further dissection of the cochlea immunohistochemistry was performed as described previously (8).

Primary antibodies used were are listed in Table 1. Primary antibodies were detected using Alexa Fluor tagged secondary antibodies 488 and 568 (Molecular Probes; 1:1000). Actin was labeled with phalloidin-555 (Sigma; 1:200). Images were obtained using a Zeiss 510 laser scanning confocal microscope with 20x (dry), 40x, or 63x oil immersion objectives.

Olfactory tissue processing, immunostaining and cell counts: Nine to 12 week old male mice were transcardially perfused in cold 0.1M PBS and 4% PFA. After dissection, epithelial tissue was post-fixed in 4% PFA for 24 hours at 4°C, and decalcified in 49.5% 2N HCL solution for two hours at room temperature. Tissue was then cryoprotected in 30% sucrose for 24 hours at 4°C, and cut into 40 µm sections on a cryostat (CM3050 S, Leica). Sections were treated with 1% NaBH4 for 15 minutes, washed 5x in TBS, and put in blocking solution (0.1% gelatin, 5% normal goat serum (NGS) and 0.5% Triton-X 100) for one hour at room temperature. Sections were then transferred to primary solution (3% NGS and 0.2% Triton-X 100) and incubated for 36-48 hours shaking at 4°C, washed 4x in TBS, and incubated in secondary solution (3% NGS and 0.2% Triton-X 100) for two hours at room temperature. Sections were then washed 4x in TBS and mounted using Vectashield mounting media with DAPI. Primary antibodies included the following: Olfactory marker protein (OMP), 1:5000 (Wako); Growth associated protein 43 (Gap-43), 1:2500 (Novus). Sections were examined using confocal microscopy (LSM510, Carl Zeiss). OMP and Gap-43 positive cells counted in single optical sections using ImageJ Cell Counter in a 300 µm region of septal epithelium from both miR-183 cluster$^{ko/ko}$ and miR-183 cluster$^{+/+}$ mice (N=4 per genotype; two sections per animal and two regions per section were counted). Data was analyzed using two-tailed, unpaired T-tests in GraphPad Prism.

Retinal flat mount imaging: Immediately following euthanization, mice were marked on ventral side of the eyes. Eyes were then removed and fixed in 4% PFA in PBS at 25˚C. After fixation for 60 minutes, a small piece of the central cornea was removed using micro scissors under a Zeiss Stemi 2000-C stereo microscope and fixation continued for another 3-4 h at 4 ˚C. The cornea and lens were removed and, with the previously marked ventral side as a guide, the ventral and dorsal sides of the retina were marked with blue and red tissue marking dye respectively before being separated from the rest of the eye cup with a brush. The retina was permeabilized in PBS containing 0.5% Triton X-100 for 10 min at room temperature, washed 3x in PBS, and blocked with ICC buffer (1x PBS with 0.2 % Tween-20, 0.5% bovine serum albumin (BSA) and 0.05% sodium azide) containing 10% BSA or goat serum for 3 hours at room temperature. After washing 1x with PBS, the retina was incubated with primary antibodies in ICC buffer with 10% BSA or goat serum for 16 hours at 4 ˚C on a rocker, washed 4x with ICC buffer (15 min each) and then incubated with secondary antibodies with DAPI (1µg/ml) in ICC buffer for 3 hours at room temperature. The retina was washed 3x in ICC buffer for 15 min each and 2x for 30 min each and then mounted in Prolong Gold mounting media (Invitrogen) before imaging on Leica SP2 confocal system.

RNA-sequencing and data analyses: DNA-free total RNA was prepared from a pool of retinas from 5 miR-183 cluster$^{KO/KO}$ or age-matched C57bl6/J control mice, by use of PureLink RNA Mini Kit and TRIzol Reagent (Life Technologies) and on-column DNase treatment with PureLink DNase (Life Technologies) according to manufacturer's instructions. RNA integrity was evaluated by 2100 Bioanalyzer (Agilent Technologies) with RIN no less than 7. RNA-seq was performed by NIH Intramural Sequencing Center (Bethesda, MD). One paired end index library from each polyA(+)-selected RNA samples was prepared. Six samples were pooled and loaded on 2 lane(s) of Illumina HiSeq 2000 Sequencer, and run as paired end index 100 base reads with a total of 40 million base read pairs per sample. Quality of RNA-seq data in FASTQ format was accessed by use of FASTQC. Differential mRNA expression between miR-183 cluster knockout mice and age-matched C57bl6/J control mice was quantified by RNA-seq data analysis using the Tuxedo package (i.e. the Tophat-Cufflinks pipeline) on the NIH Biowulf high performance computing platform. Alignment was performed by use of Tophat version 2.1.1 (Bowtie2) and the mouse10 reference genome

(NCBI) with standard parameters. Cufflinks version 2.2.1 was used to assemble the transcriptomes and CuffDiff was used to quantify the levels of gene expression in Reads Per Kilobase of transcript per Million mapped reads (RPKM). False discovery rate (FDR) value of less than or equal to 0.1 was used as the criteria for "significant" differentially regulated genes. RNA-seq data at P5, P11 and P27 of miR-183 cluster KO retina can be accessed at NCBI GEO repository, accession number GSE95852.

SI Appendix Supplementary Figures (S figures):

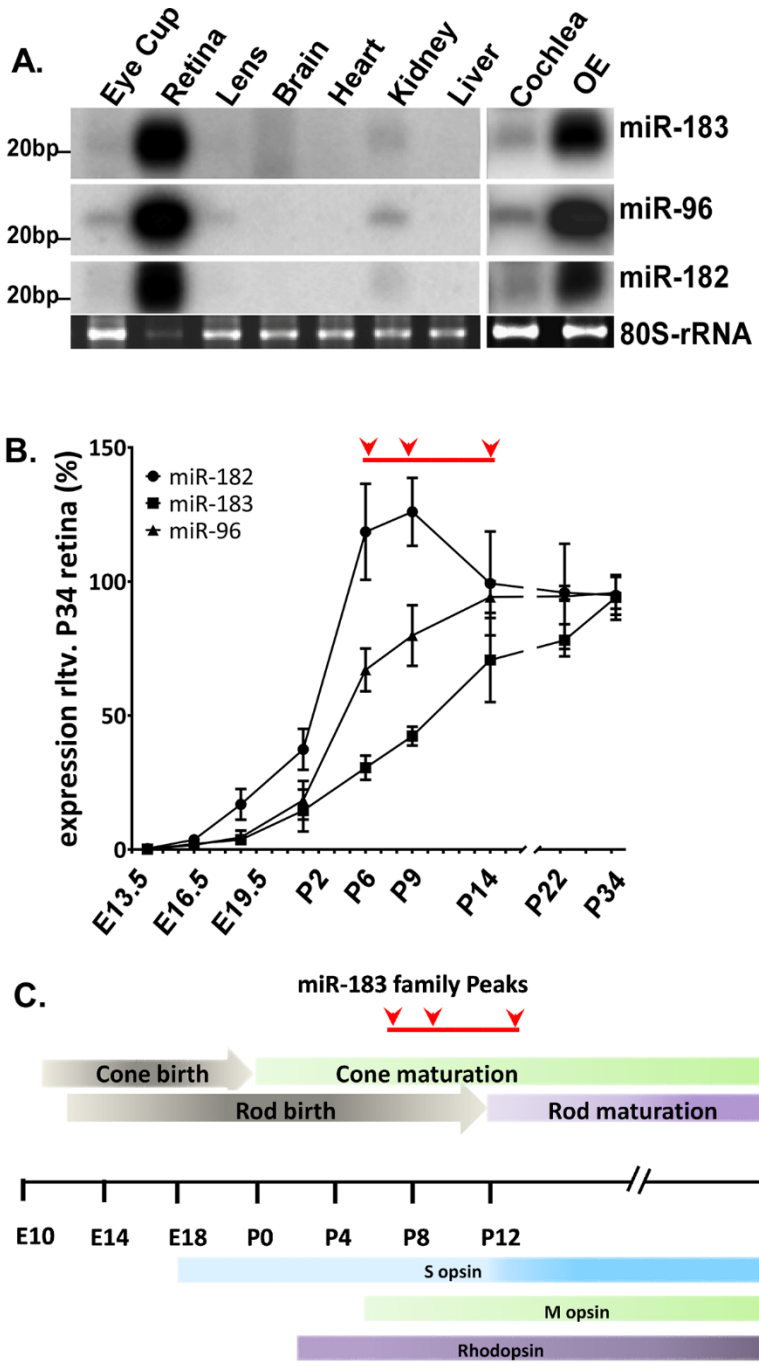

SI Appendix S1: microRNAs of miR-183 cluster is enriched in sensory receptor cells. (A) Northern blots of total RNA prepared from a panel of tissues of wild type C57B/6J mice at age P30 using P^{32}-labeled LNA probes (Exiqon) specific to miR-183, -96 and -182. OE: olfactory epithelium. (B) Temporal expression of miR-183, -96 and -182 in mouse retina by q-PCR from E13.5 to P34, a period covering normal photoreceptor genesis and maturation (error bars are STD). (C) The time

course of rapid increase of the three microRNAs coincides with that of photoreceptor maturation (9) (red arrow heads).

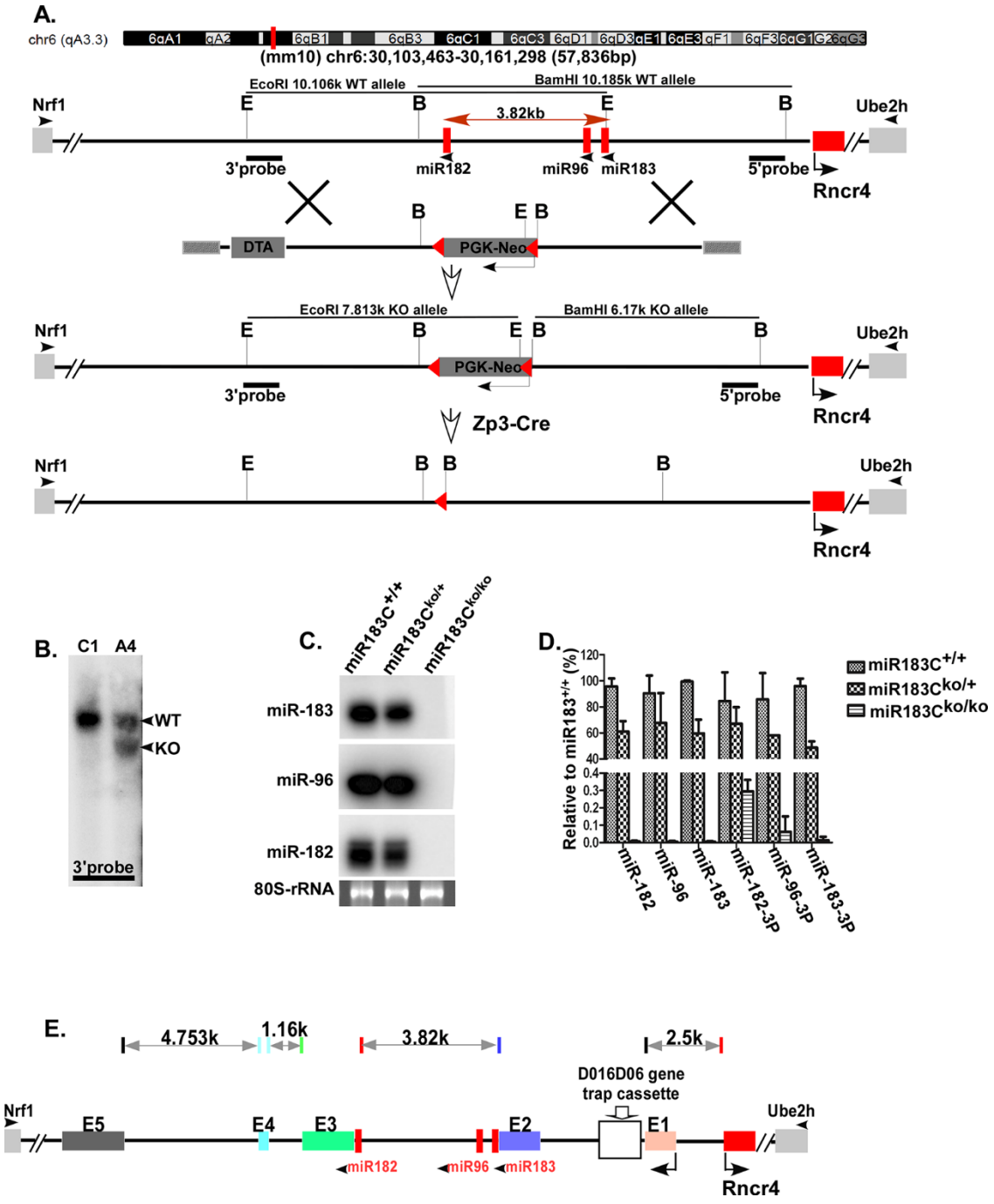

SI Appendix S2: Complete inactivation of miR-183 cluster by homologous recombination (HR) in mouse germ line. (A) Schematic representation of the mouse miR-183 cluster locus, the targeting vector, and the mutant allele. Locations of the hybridization probes (5'- and 3'- probe) for Southern blot analysis are shown. (B) Southern blot of the ES clone C1 with intended HR event as demonstrated by the presence of the 7.813kb EcoRI KO allele. (C) Northern blot showing complete absence of expression of three miRNAs encoded by miR-183 cluster from retinas of miR-183 cluster$^{KO/KO}$ mice. (D) q-PCR demonstrated expressions of the mature miRNAs, both 5P and 3P, were completely missing from retinas of miR-183 cluster$^{KO/KO}$ mice. (E) miR-183 cluster gene organization with exons (exons 3 and 4 are novel exons discovered in this study) of host gene transcripts and introns. The empty box marks the location of the gene trap cassette in ES clone D016D06 used to generate the miR-183GT allele (10), which is 2.5 kb upstream of the Rncr4 gene (red rectangle) coding for a lncRNA that positively regulates biogenesis of miR-183 cluster miRNAs (11).

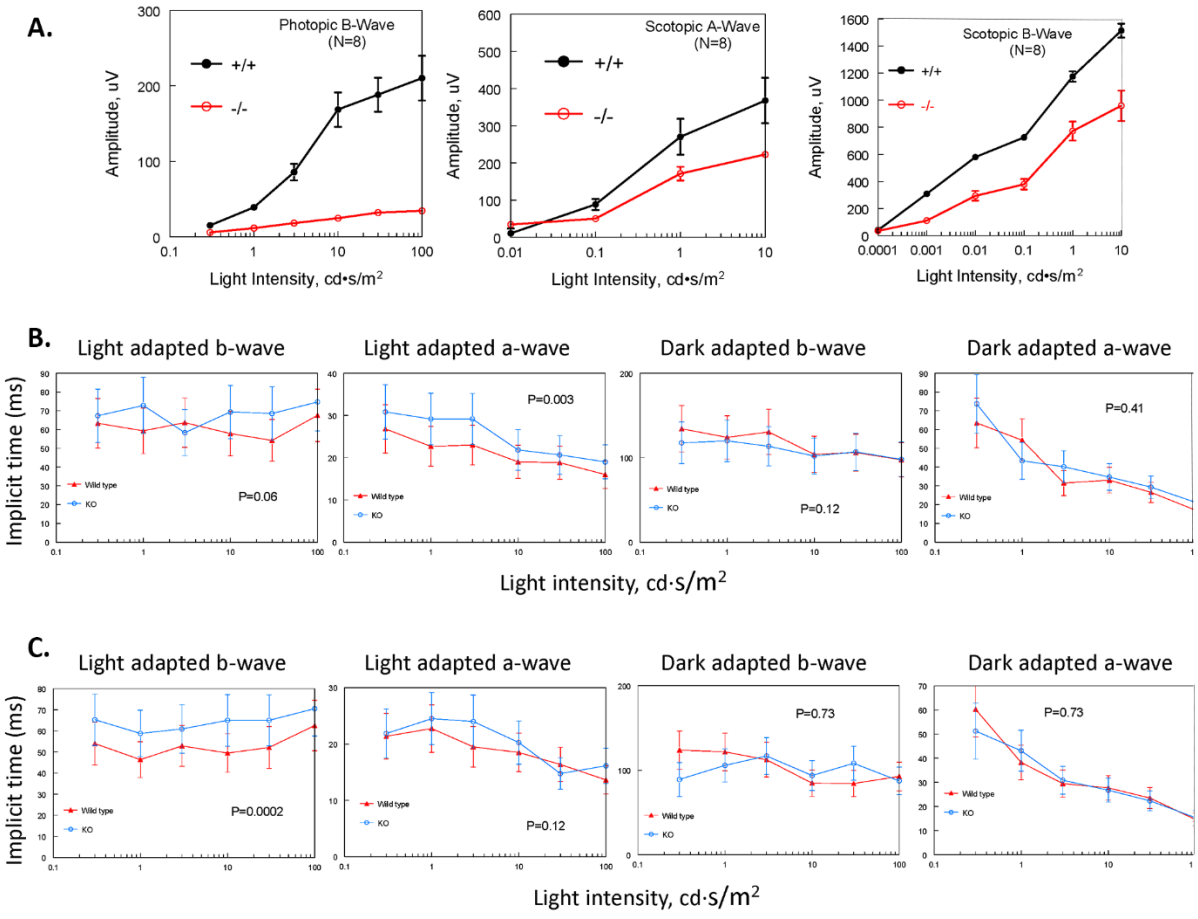

SI Appendix S3: Quantitative measurements of ERG responses. (A). Photopic and scotopic responses (amplitudes) were measured as a function of stimulus light intensities under dark and light adaptation conditions in 4-6 month old wild type and miR-183 cluster$^{KO/KO}$ mice. (B-C) Implicit times of ERG responses (both a- and b- wave) under dark and light adaptation conditions were plotted as a function of stimulus light intensities, in both wild type and miR-183 cluster$^{KO/KO}$ mice at p16 (B) and 4-6 months (C) respectively. p-values from pair-wise t-test is indicated.

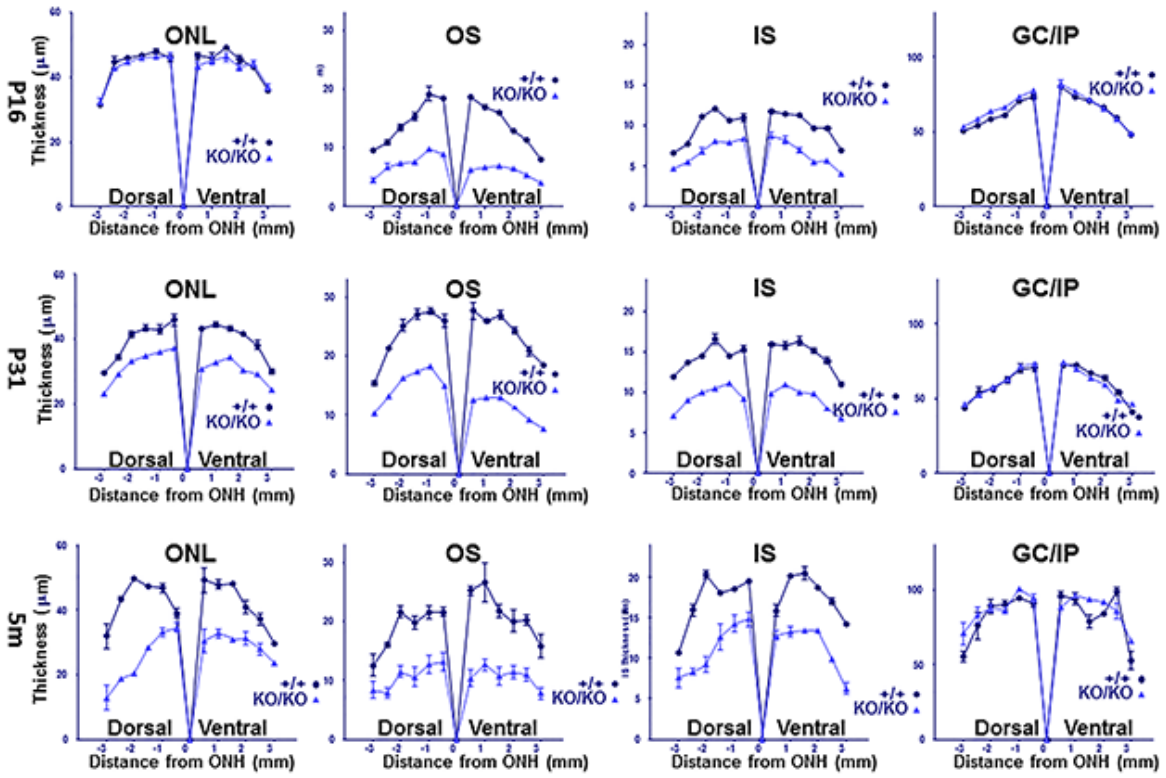

SI Appendix S4: Measurements of major retinal layers from miR-183 cluster$^{ko/ko}$ mice: Thickness of ONL, OS, IS, ganglion cell (GC)/Inner plexiform (IP) layers were measured throughout retina and plotted over distances from optical nerve head (ONH) at ages indicated. Overall thickness of the ONL remained unchanged in miR-183 cluster$^{ko/ko}$ compared to wild type controls at p16, but was significantly reduced by p31 especially in areas surrounding ONH. By 5 months, thinning of ONL progressed especially in the dorsal peripheral area. OS and IS layers

were significantly thinner than wild type in the mutant from as early as p16. GC/IP layer, however, did not show significant difference between miR-183 cluster$^{KO/KO}$ and wild type. Measurements were taken using AxioVision software (Carl Zeis,) from 0.5µm plastic sections. N=4 and Error bars are SD.

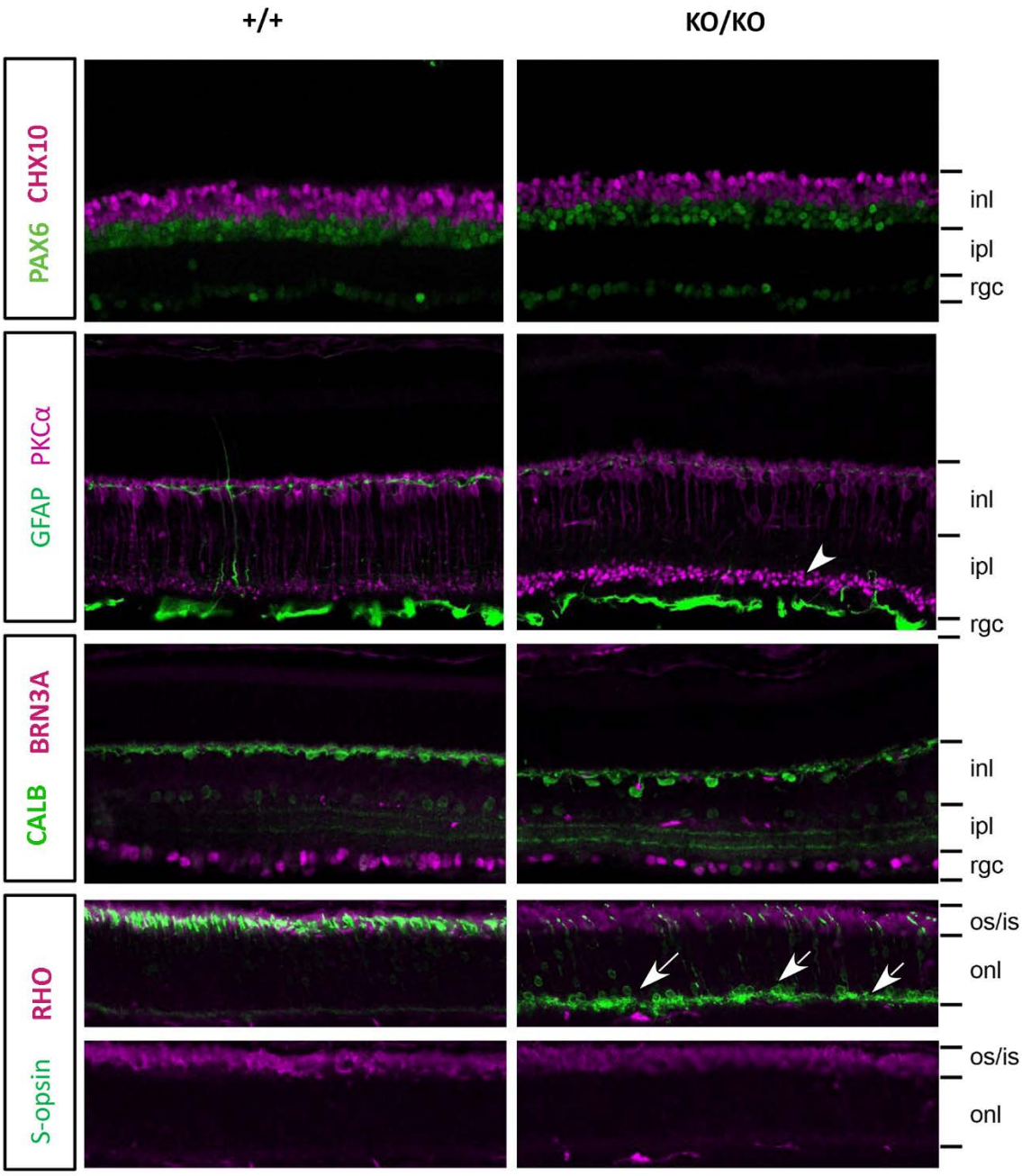

SI Appendix S5: Immunological staining of retina with a panel of marker antibodies for major cell types in the retina. Frozen sections were stained with a panel of marker antibodies: CHX10 for bipolar; PAX6 for amacrine; PKCα for rod ON bipolar; GFAP for Müller glia; CALB (Calbindin) for horizontal, BRN3A for ganglion, RHO for rod, and S-opsin for cone. At p23**,** appearances of most retina markers were unchanged in the miR-183 cluster$^{ko/ko}$ except for S-opsin, RHO and PKCα. Intense staining of S-opsin was localized to the border of ONL and OPL (arrows) of the mutant retina, where cone pedicles are normally localized. Also, there were very few mature outer segments as labeled by S-opsin in miR-183 cluster$^{ko/ko}$ retina. RHO staining in outer segments of the mutant was at a reduced level at p23 compared to wild type. In the miR-183 cluster$^{KO/KO}$ retina, PKCα, a marker specific for rod ON-bipolar cells, was more intensely labeled in the synaptic terminals compared to wild type.

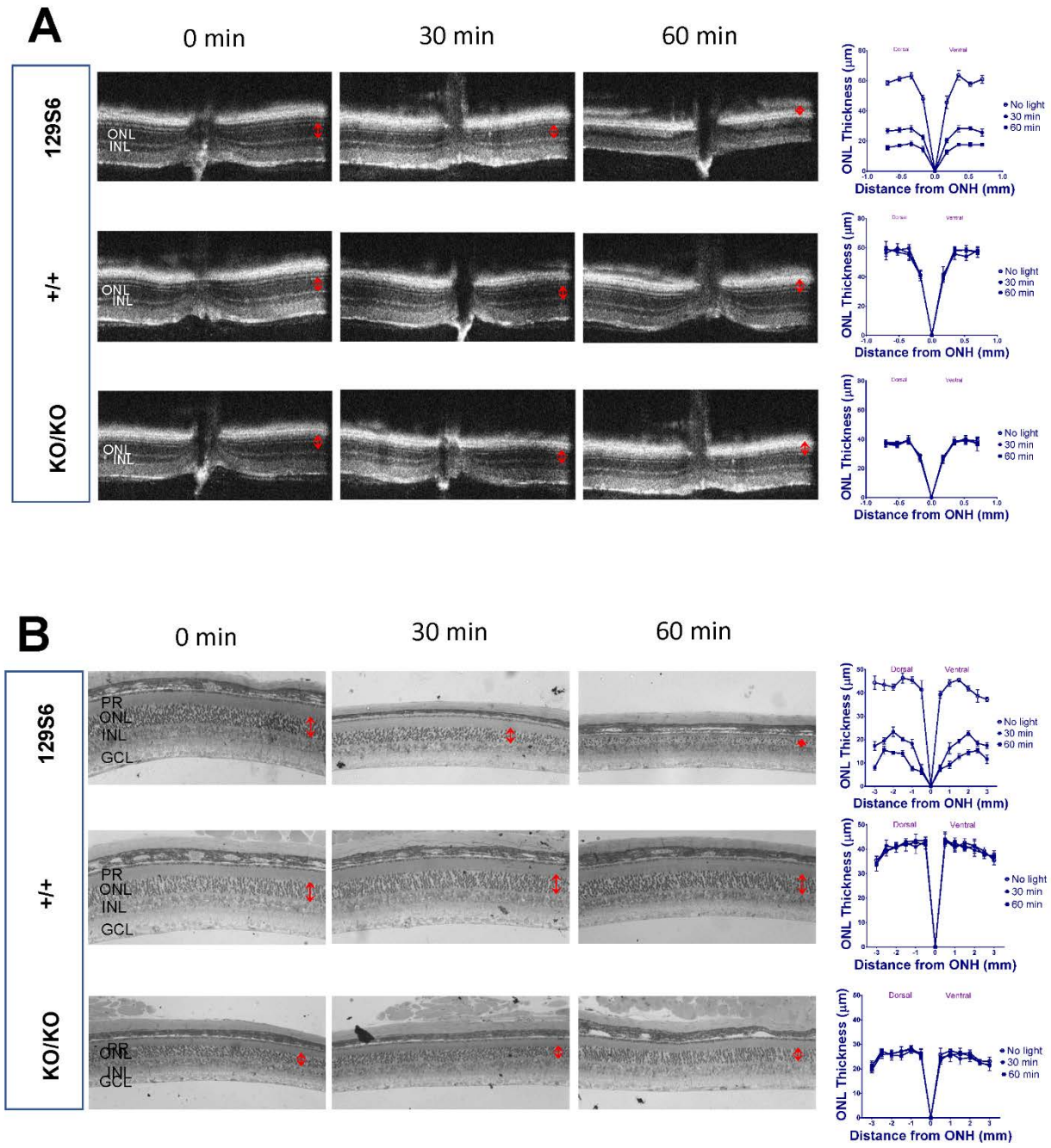

SI Appendix S6: No increase in susceptibility to light-induced retinal damage in miR-183 cluster-KO mice. Dark adapted miR-183 cluster$^{ko/ko}$ mice (2-month-old) and age-matched wild type C57B/6J and 129S6 controls were exposed to fluorescent light at 10000 lux for 0, 30 and 60 minutes respectively followed by 2 weeks of normal day/night cycles. Retinas were examined by SD-OCT (A) and H&E staining of plastic sections of 0.5μm thickness (B) and representative images were shown as indicated. In addition, thickness of ONL was measured using images from

both the OCT experiment (A) and plastic sections (B) and plotted over distances from optical nerve head (ONH). The resulting line graphs were displayed at the end of each panels. Error bars represent means ± the standard deviation (N=3). No further change of ONL thickness was observed in the miR-183 cluster KO retina upon light damage by either OCT ($p=0.19$ and 0.22, respectively, when 30 min and 60 min treatment is compared with no-light control) or H&E staining ($p=0.08$ when either 30 min or 60 min treatment is compared with no-light control). Similarly, no further thinning of ONL was observed in C57B/6J wild type mouse retina upon light damage by either OCT ($p=0.10$ and 0.17, respectively, when 30 min and 60 min treatment is compared with no-light control) or H&E staining ($p=0.34$ and 0.26, respectively, when 30 min and 60 min treatment is compared with no-light control). In contrast, 129S6 mice underwent significant retinal degeneration under the same light exposure ($p<0.01$ with either 30 min or 60 min light exposure compared to no-light control in measurements with either OCT or plastic section images). The p values were calculated using the pair-wise two-tailed T-test.

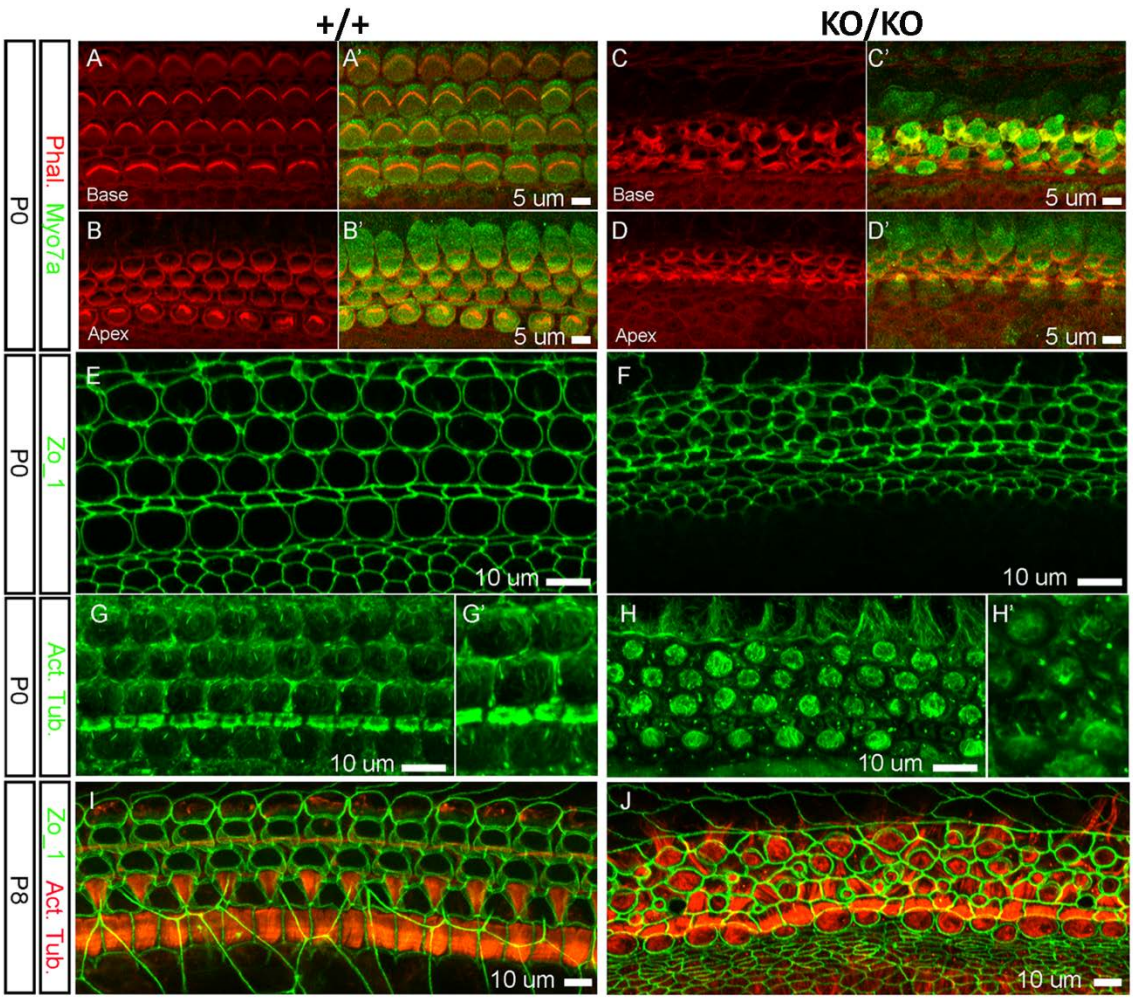

SI Appendix S7: Appearance of hair cell markers in cochlea. (A-D): Immunofluorescence for a hair cell marker Myo7a (green) and F-actin (phalloidin, red) in cochlea whole mounts at P0. In miR-183 cluster$^{+/+}$ mice the specification of hair cells into one row of inner hair cells, and three rows of outer hair cells separated by support cells is clearly defined and stereocilia bundles (F-actin) are uniformly orientated. In miR-183 cluster$^{KO/KO}$ cochlea, maturation and specification of hair cells (and support cells) looks abnormal or delayed. (E-F): Immunofluorescence for Zo_1 in cochlea whole mounts at P0. Abnormalities in the cellular rearrangements in the KO cochlea are highlighted. (G-H): Immunofluorescence for acetylated tubulin in cochlea whole mounts at P0. Note up-regulation and disorganization of stable microtubules in hair cells vs miR-183 cluster$^{+/+}$. (I-J) Immunofluorescence for Zo_1 and acetylated tubulin in P8 cochlea shows a similar pattern to P0.

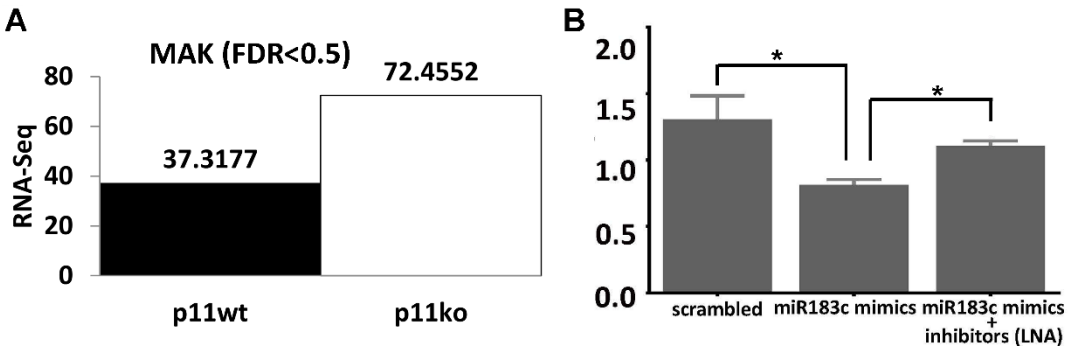

SI Appendix S8: Mak is a potential target for miR-183 cluster. (A) RNA-seq (Reads Per Kilobase of transcript per Million mapped reads (RPKM)) analysis showed increased Mak transcript in the miR-183 cluster$^{KO/KO}$ retina at p11 (FDR<0.5). (B) Luciferase assay showing that 3'-UTR of Mak gene can directly interact with mixed mimetics of miR-183 cluster microRNAs. 3'-UTR of mouse Mak gene was cloned into the firefly luciferase reporter vector. HEK293 cells were co-transfected with reporter plasmids and a mixture of mouse miR-182, miR-183, and miR-96 mimetics at molar ratios of 1:1:2. Luciferase activity was measured as the ratio of firefly vs. renilla luciferase activities. Compared to transfection of scrambled small RNAs (scrambled), a decrease in luciferase activity is observed in cells transfected with miR-183 cluster mimics, which was reversed by LNA inhibitor specific to the miR-183 cluster microRNAs. Data represent three independent experiments ($p<0.05$)

SI Appendix Tables

S Table 1: Candidate effector genes; references (12-42)

S Table 2: Expressed targets of miR-183 cluster miRNAs at P5, P11 and P27

SI Appendix references

1. Thomas KR & Capecchi MR (1987) Site-directed mutagenesis by gene targeting in mouse embryo-derived stem cells. *Cell* 51(3):503-512.
2. Muyrers JP*, et al.* (2004) ET recombination: DNA engineering using homologous recombination in E. coli. *Methods in molecular biology (Clifton, N.J.)* 256:107-121.
3. Lewandoski M, Wassarman KM, & Martin GR (1997) Zp3-cre, a transgenic mouse line for the activation or inactivation of loxP-flanked target genes specifically in the female germ line. *Current biology : CB* 7(2):148-151.
4. Varallyay E, Burgyan J, & Havelda Z (2008) MicroRNA detection by northern blotting using locked nucleic acid probes. *Nature protocols* 3(2):190-196.

5. Yang J*, et al.* (2002) Rootletin, a novel coiled-coil protein, is a structural component of the ciliary rootlet. *The Journal of cell biology* 159(3):431-440.
6. Willott JF (2006) Measurement of the auditory brainstem response (ABR) to study auditory sensitivity in mice. *Current protocols in neuroscience / editorial board, Jacqueline N. Crawley ... [et al.]* Chapter 8:Unit8 21B.
7. Yang M & Crawley JN (2009) Simple behavioral assessment of mouse olfaction. *Current protocols in neuroscience / editorial board, Jacqueline N. Crawley ... [et al.]* Chapter 8:Unit 8 24.
8. May-Simera H & Kelley MW (2012) Examining planar cell polarity in the mammalian cochlea. *Methods in molecular biology* 839:157-171.
9. Swaroop A, Kim D, & Forrest D (2010) Transcriptional regulation of photoreceptor development and homeostasis in the mammalian retina. *Nature reviews. Neuroscience* 11(8):563-576.
10. Lumayag S*, et al.* (2013) Inactivation of the microRNA-183/96/182 cluster results in syndromic retinal degeneration. *Proceedings of the National Academy of Sciences of the United States of America* 110(6):E507-516.
11. Krol J*, et al.* (2015) A network comprising short and long noncoding RNAs and RNA helicase controls mouse retina architecture. *Nature communications* 6:7305.
12. Seo S*, et al.* (2010) BBS6, BBS10, and BBS12 form a complex with CCT/TRiC family chaperonins and mediate BBSome assembly. *Proceedings of the National Academy of Sciences of the United States of America* 107(4):1488-1493.
13. Davis EE*, et al.* (2011) TTC21B contributes both causal and modifying alleles across the ciliopathy spectrum. *Nature genetics* 43(3):189-196.
14. Bachmann-Gagescu R*, et al.* (2015) The Ciliopathy Protein CC2D2A Associates with NINL and Functions in RAB8-MICAL3-Regulated Vesicle Trafficking. *PLoS genetics* 11(10):e1005575.
15. Boldt K*, et al.* (2011) Disruption of intraflagellar protein transport in photoreceptor cilia causes Leber congenital amaurosis in humans and mice. *The Journal of clinical investigation* 121(6):2169-2180.
16. Gao J*, et al.* (2002) Progressive photoreceptor degeneration, outer segment dysplasia, and rhodopsin mislocalization in mice with targeted disruption of the retinitis pigmentosa-1 (Rp1) gene. *Proceedings of the National Academy of Sciences of the United States of America* 99(8):5698-5703.
17. Sato T*, et al.* (2014) Rab8a and Rab8b are essential for several apical transport pathways but insufficient for ciliogenesis. *Journal of cell science* 127(Pt 2):422-431.
18. Schober JM, Kwon G, Jayne D, & Cain JM (2012) The microtubule-associated protein EB1 maintains cell polarity through activation of protein kinase C. *Biochemical and biophysical research communications* 417(1):67-72.
19. Hidalgo-de-Quintana J*, et al.* (2015) The Leber congenital amaurosis protein AIPL1 and EB proteins co-localize at the photoreceptor cilium. *PloS one* 10(3):e0121440.
20. Gall Troselj K, Novak Kujundzic R, & Ugarkovic D (2016) Polycomb repressive complex's evolutionary conserved function: the role of EZH2 status and cellular background. *Clinical epigenetics* 8:55.
21. Yu J*, et al.* (2011) KASH protein Syne-2/Nesprin-2 and SUN proteins SUN1/2 mediate nuclear migration during mammalian retinal development. *Human molecular genetics* 20(6):1061-1073.
22. Michalakis S*, et al.* (2005) Impaired opsin targeting and cone photoreceptor migration in the retina of mice lacking the cyclic nucleotide-gated channel CNGA3. *Investigative ophthalmology & visual science* 46(4):1516-1524.
23. Sakamoto K, McCluskey M, Wensel TG, Naggert JK, & Nishina PM (2009) New mouse models for recessive retinitis pigmentosa caused by mutations in the Pde6a gene. *Human molecular genetics* 18(1):178-192.

24. Cheng LL*, et al.* (2016) Novel mutations in PDE6B causing human retinitis pigmentosa. *International journal of ophthalmology* 9(8):1094-1099.
25. Dvir L*, et al.* (2010) Autosomal-recessive early-onset retinitis pigmentosa caused by a mutation in PDE6G, the gene encoding the gamma subunit of rod cGMP phosphodiesterase. *American journal of human genetics* 87(2):258-264.
26. Grau T*, et al.* (2011) Decreased catalytic activity and altered activation properties of PDE6C mutants associated with autosomal recessive achromatopsia. *Human molecular genetics* 20(4):719-730.
27. Brennenstuhl C*, et al.* (2015) Targeted ablation of the Pde6h gene in mice reveals cross-species differences in cone and rod phototransduction protein isoform inventory. *The Journal of biological chemistry* 290(16):10242-10255.
28. Dutta N & Seo S (2016) RPGR, a prenylated retinal ciliopathy protein, is targeted to cilia in a prenylation- and PDE6D-dependent manner. *Biology open* 5(9):1283-1289.
29. Chen CK (2002) Recoverin and rhodopsin kinase. *Advances in experimental medicine and biology* 514:101-107.
30. Shi Z*, et al.* (2011) Vsx1 regulates terminal differentiation of type 7 ON bipolar cells. *The Journal of neuroscience : the official journal of the Society for Neuroscience* 31(37):13118-13127.
31. Dryja TP*, et al.* (2005) Night blindness and abnormal cone electroretinogram ON responses in patients with mutations in the GRM6 gene encoding mGluR6. *Proceedings of the National Academy of Sciences of the United States of America* 102(13):4884-4889.
32. Kevany BM*, et al.* (2013) Structural and functional analysis of the native peripherin-ROM1 complex isolated from photoreceptor cells. *The Journal of biological chemistry* 288(51):36272-36284.
33. Yang J, Adamian M, & Li T (2006) Rootletin interacts with C-Nap1 and may function as a physical linker between the pair of centrioles/basal bodies in cells. *Molecular biology of the cell* 17(2):1033-1040.
34. Liu Q, Lyubarsky A, Skalet JH, Pugh EN, Jr., & Pierce EA (2003) RP1 is required for the correct stacking of outer segment discs. *Investigative ophthalmology & visual science* 44(10):4171-4183.
35. Omori Y*, et al.* (2010) Negative regulation of ciliary length by ciliary male germ cell-associated kinase (Mak) is required for retinal photoreceptor survival. *Proceedings of the National Academy of Sciences of the United States of America* 107(52):22671-22676.
36. Rachel RA*, et al.* (2012) Combining Cep290 and Mkks ciliopathy alleles in mice rescues sensory defects and restores ciliogenesis. *The Journal of clinical investigation* 122(4):1233-1245.
37. Chen C*, et al.* (2015) Characterization of Cep85 - a new antagonist of Nek2A that is involved in the regulation of centrosome disjunction. *Journal of cell science* 128(20):3837.
38. Yamashita T*, et al.* (2009) Essential and synergistic roles of RP1 and RP1L1 in rod photoreceptor axoneme and retinitis pigmentosa. *The Journal of neuroscience : the official journal of the Society for Neuroscience* 29(31):9748-9760.
39. Graser S*, et al.* (2007) Cep164, a novel centriole appendage protein required for primary cilium formation. *The Journal of cell biology* 179(2):321-330.
40. Khateb S*, et al.* (2014) A homozygous nonsense CEP250 mutation combined with a heterozygous nonsense C2orf71 mutation is associated with atypical Usher syndrome. *Journal of medical genetics* 51(7):460-469.
41. Wu Q*, et al.* (2012) Cep57, a NEDD1-binding pericentriolar material component, is essential for spindle pole integrity. *Cell research* 22(9):1390-1401.
42. Kypri E*, et al.* (2014) The nucleotide-binding proteins Nubp1 and Nubp2 are negative regulators of ciliogenesis. *Cellular and molecular life sciences : CMLS* 71(3):517-538.

SI Appendix S Table 1: miR-183 cluster candidate effector genes

	P5				P11				P27							
Gene	WT	KO	KO /WT	q	WT	KO	KO /WT	q	WT	KO	KO /WT	q	Relevant GO terms	Predicted target	Seed match type	References (SI Appendix)
Ezh2	9.3	27.7	3.0	0.04	3.4	6.4	1.8	1.00	5.9	4.7	0.8	1.00	generate repressive histone mark H3K27me3 at target genes	no	N/A	(20)
Syne2	9.6	15.0	1.6	1.00	9.0	13.7	1.5	1.00	21.6	18.1	0.8	1.00	LINC complex/ nuclear envelope	miR-96/182-5P	7-mer-A1/7-merA1; both conserved	(21)
Kif2a	19.7	26.3	1.3	1.00	24.0	28.2	1.2	1.00	29.6	29.1	1.0	1.00	LINC complex/ microtubule cytoskeleton	miR-182/183-5p	8mer/7mer-m8; both conserved	(21)
Dync1i1	4.1	4.3	1.1	1.00	17.0	20.6	1.2	1.00	26.9	30.2	1.1	1.00	LINC complex/ dynein complex	no	N/A	(21)
Cnga3	2.8	2.9	1.0	1.00	2.8	3.0	1.1	1.00	3.9	2.8	0.7	1.00	Cone cyclic nucleotide-gated channel	no	N/A	(22)
Opn1sw	52.4	34.9	0.7	1.00	83.8	120.5	1.4	1.00	185.1	160.8	0.9	1.00	Cone opsin/phototransduction	no	N/A	
Opn1mw	0.2	0.1	0.9	1.00	34.0	27.8	0.8	1.00	87.9	64.4	0.7	1.00	Cone opsin/phototransduction	no	N/A	
Rho	249.0	94.5	0.4	0.04	5064.0	3596.4	0.7	1.00	9698.5	7825.3	0.8	1.00	Rod opsin/phototransduction/ ciliary membrane	no	N/A	(29)
Pde6a	10.3	7.3	0.7	1.00	263.8	310.6	1.2	1.00	767.1	630.5	0.8	1.00	Catalytic subunit of Pde6 in Rod /phototransduction/rho-mediated signaling pathway	no	N/A	(23)
Pde6b	156.6	123.4	0.8	1.00	540.5	551.5	1.0	1.00	818.3	655.8	0.8	1.00	Catalytic subunit of Pde6 in Rod /phototransduction/rho-mediated signaling pathway	no	N/A	(24)
Pde6g	140.1	116.6	0.8	1.00	726.0	723.6	1.0	1.00	921.0	829.6	0.9	1.00	Inhibitory subunit of Pde6 in Rod /phototransduction/rho-mediated signaling pathway	no	N/A	(25)
Pde6c	10.2	5.3	0.5	1.00	38.6	16.4	0.4	0.61	48.6	33.7	0.7	1.00	Catalytic subunit of Pde6 in Cone /phototransduction	no	N/A	(26)

Pde6h	**52.3**	**7.0**	**0.1**	**0.04**	**89.9**	**28.3**	**0.3**	**0.48**	**91.2**	**62.1**	**0.7**	**1.00**	**Inhibitory subunit of Pde6 in Cone /phototransduction**	**no**	**N/A**	**(27)**
Pde6d	**22.7**	**35.9**	**1.6**	**1.00**	**36.2**	**50.8**	**1.4**	**1.00**	**54.1**	**53.0**	**1.0**	**1.00**	**prenyl-binding protein/RPGR binding**	**no**	**N/A**	**(28)**
Rcvrn	**29.7**	**18.1**	**0.6**	**1.00**	**376.5**	**493.6**	**1.3**	**1.00**	**499.3**	**503.6**	**1.0**	**1.00**	**Photoreceptor/ phototransduction**	**no**	**N/A**	**(29)**
Prkca	**15.4**	**14.8**	**1.0**	**1.00**	**54.4**	**55.1**	**1.0**	**1.00**	**62.0**	**49.2**	**0.8**	**1.00**	**ON-bipolar cell**	**miR-183-5P**	**7mer-m8; conserved**	
Vsx1	**1.3**	**5.7**	**4.4**	**0.04**	**6.6**	**9.0**	**1.4**	**1.00**	**10.9**	**8.2**	**0.8**	**1.00**	**ON-bipolar cell/homeobox gene/transcription factor**	**no**	**N/A**	**(30)**
Grm6	**1.1**	**7.7**	**7.2**	**0.04**	**27.1**	**52.8**	**1.9**	**1.00**	**36.4**	**28.8**	**0.8**	**1.00**	**ON-bipolar cell/glutamate receptor**	**no**	**N/A**	**(31)**
Rom1	**349.0**	**216.3**	**0.6**	**1.00**	**696.8**	**574.3**	**0.8**	**1.00**	**844.8**	**723.5**	**0.9**	**1.00**	**Ciliary /photoreceptor disc membrane/ ciliary membrane**	**no**	**N/A**	**(32)**
Crocc	**34.7**	**53.6**	**1.5**	**1.00**	**38.9**	**57.6**	**1.5**	**1.00**	**63.6**	**53.0**	**0.8**	**1.00**	**Ciliary / major rootlet structural gene**	**no**	**N/A**	**(5, 33)**
Rp1	**164.4**	**119.2**	**0.7**	**1.00**	**385.1**	**274.7**	**0.7**	**1.00**	**450.2**	**388.2**	**0.9**	**1.00**	**Ciliary / photoreceptor connecting cilium**	**no**	**N/A**	**(16, 34)**
Mak	**27.8**	**54.1**	**1.9**	**0.74**	**37.3**	**72.5**	**1.9**	**0.95**	**100.7**	**111.3**	**1.1**	**1.00**	**Ciliary / Axoneme /negatively regulator of OS length**	**miR-96/182-5P**	**8mer/7mer-1A; both conserved**	**(35)**
Mkks	**4.2**	**7.3**	**1.7**	**1.00**	**4.9**	**13.9**	**2.8**	**0.88**	**14.3**	**14.7**	**1.0**	**1.00**	**Ciliary /basal body/McKusick-Kaufman syndrome gene/ciliogenesis**	**no**	**N/A**	**(36)**
Bbs10	**1.6**	**3.7**	**2.3**	**1.00**	**2.4**	**6.0**	**2.5**	**1.00**	**7.1**	**6.9**	**1.0**	**1.00**	**Ciliary /basal body/Bardet-Biedl syndrome 10/BBSome assembly/vesicle trafficking through a Rab8**	**no**	**N/A**	**(12)**
Ttc21b	**4.2**	**11.0**	**2.6**	**0.38**	**4.8**	**11.7**	**2.4**	**0.65**	**13.5**	**13.0**	**1.0**	**1.00**	**Ciliary /basal body & axoneme/retrograde IFP**	**no**	**N/A**	**(13)**
Bbs12	**5.1**	**9.1**	**1.8**	**1.00**	**7.7**	**17.1**	**2.2**	**0.95**	**22.3**	**23.5**	**1.1**	**1.00**	**Ciliary /basal body/BBSome assembly/vesicle trafficking Rab8**	**no**	**N/A**	**(12)**
Cc2d2a	**10.2**	**17.0**	**1.7**	**1.00**	**11.5**	**23.6**	**2.0**	**0.86**	**32.7**	**26.0**	**0.8**	**1.00**	**Ciliary /Transition zone/docking ciliary vesicular trafficking**	**no**	**N/A**	**(14)**
Lca5	**15.5**	**20.0**	**1.3**	**1.00**	**18.5**	**30.7**	**1.7**	**1.00**	**27.1**	**29.5**	**1.1**	**1.00**	**Ciliary / connecting cilium/ TFT/ interacting with complex B**	**no**	**N/A**	**(15)**

Rab8b	**23.3**	**15.4**	**0.7**	**1.00**	**16.9**	**10.5**	**0.6**	**1.00**	**8.8**	**9.3**	**1.1**	**1.00**	**Ciliary /Small GTP-binding protein/ IFP /Ciliogenesis & elongation of ciliary membranes**	**miR-183-5P**	**8mer; conserved**	**(17)**
Mapre1	**69.2**	**58.8**	**0.8**	**1.00**	**48.9**	**30.3**	**0.6**	**1.00**	**17.2**	**18.1**	**1.1**	**1.00**	**Ciliary / connecting cilium/ linking microtubule to actin**	**miR-96/182-5P**	**7mer-A1/7mer-A1; both conserved**	**(18, 19)**
Cep85	**11.0**	**17.7**	**1.6**	**1.00**	**8.8**	**16.0**	**1.8**	**1.00**	**26.1**	**19.1**	**0.7**	**1.00**	**Ciliary /Centrosome/centrosome disjunction**	**no**	**N/A**	**(37)**
Rp1l1	**21.4**	**36.7**	**1.7**	**1.00**	**62.2**	**106.9**	**1.7**	**1.00**	**137.5**	**131.0**	**1.0**	**1.00**	**Ciliary /connecting cilium/OS morphogenesis**	**no**	**N/A**	**(38)**
Cep164	**7.0**	**7.5**	**1.1**	**1.00**	**6.7**	**11.3**	**1.7**	**1.00**	**27.3**	**21.0**	**0.8**	**1.00**	**Ciliary /Distal appendages mother centriole/initiation ciliogenesis**	**no**	**N/A**	**(39)**
Cep250	**10.2**	**14.1**	**1.4**	**1.00**	**10.7**	**16.5**	**1.5**	**1.00**	**29.6**	**18.9**	**0.6**	**0.92**	**Ciliary /Centrosome/cohesion of two centrioles and basal body/interact with rootletin (Crocc)**	**miR-182-5P**	**8mer; conserved**	**(40)**
Cep57	**29.5**	**21.9**	**0.7**	**1.00**	**24.8**	**14.0**	**0.6**	**1.00**	**15.8**	**14.5**	**0.9**	**1.00**	**Ciliary /Centrosome/bundle microtubules**	**no**	**N/A**	**(41)**
Nubp2	**28.0**	**19.5**	**0.7**	**1.00**	**26.9**	**14.7**	**0.5**	**1.00**	**15.9**	**15.2**	**1.0**	**1.00**	**Ciliary /Centrioles/ciliogenesis**	**no**	**N/A**	**(42)**

Candidate effector genes discussed throughout the manuscript are included here with mRNA expression levels determined by RNA-seq using RNA obtained from P5, P11, and P27 whole retinas (5 mice used for each age). Mutant vs wild type RPKM values are shown as well as KO/WT ratios with corresponding q (FDR) values. In addition, seed binding information for predicted targets of miR-183 cluster microRNAs along with relevant GO terms of all effector genes including those indirectly regulated by miR-183 cluster are listed. Reference numbers (SI Appendix) are listed in the last column.